Results in Engineering 21 (2024) 101824

Contents lists available at ScienceDirect

Results in Engineering

journal homepage: www.sciencedirect.com/journal/results-in-engineering

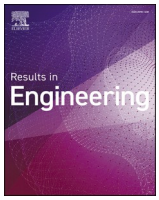

# Efficient electrochemical conversion of $CO_2$ into formic acid using colloidal NiCo@rGO catalyst

Muhammad Arsalan [a], Dina Ewis [a], Muneer M. Ba-Abbad [a], Mazen Khaled [b], Abdulkarem Amhamed [c], Muftah H. El-Naas [a,*]

[a] Gas Processing Center, College of Engineering, Qatar University, P.O.Box 2713, Doha, Qatar
[b] Department of Chemistry and Earth Sciences, College of Arts and Sciences, Qatar University, P.O.Box 2713, Doha, Qatar
[c] Qatar Environment & Energy Research Institute, Hamad Bin Khalifa University, Education City, Doha, Qatar

ARTICLE INFO

*Keywords:*
Electrochemical conversion
NiCo@rGO
$CO_2$ reduction
Formic acid

ABSTRACT

A simple approach was used to synthesize a catalyst based on colloidal NiCo with rGO support. The catalyst was uniformly deposited on acid-treated Sn foil using drop-casting method. The prepared NiCo@rGO catalyst was characterized using X-ray diffraction (XRD), scanning electron microscopy (SEM), transmission electron microscopy (TEM), and X-ray photoelectron spectroscopy (XPS). The XRD measurements confirmed the development of a homogenously immersed structure with a specific NiCo composition. The different ratios of Ni and Co in the NiCo@rGO catalyst were further confirmed by XPS and SEM-EDX. The catalyst was tested for the electrochemical reduction of $CO_2$ to produce formic acid (HCOOH) and resulted in a significantly higher faradaic efficiency at −50 mA current compared to the simple Co nanoparticle, rGO, Sn foil, Ni nanoparticles, and NiCo composite. The colloidal NiCo bimetallic structure, combined with the rGO support on the treated Sn foil, played an important role in enhancing the catalytic activity and selectivity towards formic acid. When comparing the NiCo@rGO catalyst with other catalysts, especially Ni, Co, Sn foil, NiCo, and rGO, the NiCo@rGO catalyst showed superior $CO_2$ electrochemical chemical reduction performance. The results suggest that the synergic effect of combining Ni with Co along with using acid-treated Sn foil as a support is responsible for the high activity towards formic acid production. The experimental results demonstrated the formation of formic acid with low energy consumption and good faradic efficiency.

## 1. Introduction

Carbon dioxide ($CO_2$) is produced at a faster rate than it has been consumed throughout the past century as a result of human industrial growth [1]. The rapid increase in atmospheric $CO_2$ concentration is a major contributor to climate change [2,3]. Electrochemical reduction of carbon dioxide offers a potentially long-term solution to this problem [4] and could results in the production of value-added products, including methanol, ethanol, methane, and some other valuable chemicals [5–7]. Formic acid (HCOOH), or formate (HCOO), depending on pH value, is one of the most reliable chemicals [8,9]. The annual volume of the formate/formic acid market is predicted to reach one million tons by the year 2030 [10]. There are a number of applications for formic acid and formate in the pharmaceutical, pesticide, and textile industries [11,12]. Additionally, formic acid is extensively used as a hydrogen carrier, as it is known for its ability to hold a high content of hydrogen [13]. Rhodium-based catalysts were the first to be utilized to reduce $CO_2$ to formic acid electrochemically and showed excellent formic acid Faradic efficiency (FE). Recently, Iridium-based materials showed high FE values, and ruthenium-based catalytic materials have also been deployed with the resulting FE values [14]. The Sn and SnOx are the most extensively used materials for electrochemical reduction of $CO_2$ into formic acid, among other metals such as indium, lead, mercury, silver, and platinum, which are effective in catalyzing $CO_2$RR ($CO_2$ reduction reaction) to formic acid [15–20]. The electrocatalytic efficiency of $CO_2$RR electrodes is typically improved by combining another metal or N-doped carbon materials due to the higher conductivity and more electrochemically active surface area [21–23]. Composites based on metals often show higher selectivity and better performance toward formic acid [24]. Although precious metals, such as Pd and Pt, have been known to be effective for $CO_2$ reduction reactions, it is rather difficult to expand their application on a large scale due to limited resources [25,

* Corresponding author.
*E-mail address:* muftah@qu.edu.qa (M.H. El-Naas).

https://doi.org/10.1016/j.rineng.2024.101824
Received 23 October 2023; Received in revised form 1 January 2024; Accepted 22 January 2024
Available online 1 February 2024

26]. For electrochemical conversion applications, the development of new techniques for the fabrication of nano-sized, non-precious earth's abundant metals is important [27]. Recently, some transition metals have attracted attention as potentially useful simple catalytic materials for the electrochemical conversion of carbon dioxide into formic acid [28,29].

Researchers have recently developed some earth-abundant transition metal compounds that show improved electrocatalytic activity for electrochemical reactions (such as formic acid production and oxygen reduction reactions) [30–32]. The transition metals can be utilized to change the surface structure and electronic state due to their long-chain chemical structure [33]. Therefore, it is appropriate to consider that transition metals, through their surface-modifying actions, may improve electrocatalytic activity [34]. When compared to precious metallic complexes, research on the electrochemical activity and selectivity of simple transition metals is insufficient in the context of $CO_2$ reduction electrocatalysts [35]. The challenge of establishing appropriate, moderate synthetic conditions is one of the reasons. A significant amount of work has to be done to get earth abundant transition metals suitable for selective electrochemical reduction processes. The transition metal oxide materials present some potential as a catalyst for electrochemical conversion of $CO_2$ into formic acid, and recent studies have demonstrated that the catalytic activity of non-precious metal-based catalysts may be considerably improved by doping or producing binary metal combinations [36]. Materials composed of a single metal oxide exhibit low electrocatalytic activity and selectivity [37,38]. Due to a synergic effect, the electrochemical activity of binary transition metal oxides is increased over that of single metal oxides [39,40]. There are a variety of methods for preparing metal oxide electrocatalysts, including hydrothermal, anodization, and co-precipitation [41]. The simple and easy technique is the colloidal method, which employs a homogenous combination of two precursors with a pore size between 1 and 1000 nm. The electrochemical reduction of carbon dioxide into formic acid using a colloidal metal-based material has the potential to be a safe, cost-effective, and environmentally friendly process [42]. Additionally, the electrochemical capacity and strong conduction activity of the colloidal metal-based material for the electrochemical reduction of $CO_2$ into value-added products are improved over those of simple NiOx and CoOx [43,44]. Therefore, it is important to create a colloidal NiCo-based material with high faradic efficiency, low energy consumption, and high selectivity for the electrochemical conversion of $CO_2$ into value-added products. The rGO support will be helpful in the preparation of catalysts as mentioned in the literature [45]. In long-term electrochemical applications, the colloidal technique is efficient in reducing the overpotential, increasing conductivity, and maintaining stable performance without losing catalytic activity [46]. Therefore, it is crucial to create a bimetallic catalyst using substances like nickel and cobalt that can electrochemically reduce $CO_2$ into formic acid at a low cost and with high efficiency [47]. The use of electrochemical reduction of $CO_2$ into formic acid depends on the development of Ni-based materials with superior electrochemical characteristics [48].

The current work presents a novel approach for the synthesis of a colloidal NiCo-based catalyst with rGO support on an acid-treated Sn foil that exhibits a homogeneously immersed structure. The colloidal NiCo nanocomposite is an alternative way of using earth abundant transition metals for the electrochemical reduction of $CO_2$ into value-added products. Through colloidal NiCo based material, high efficiency of $CO_2$ reduction process can be achieved. The colloidal NiCo@rGO catalyst can significantly improve the electrochemical activity for carbon dioxide conversion and show efficient reduction of carbon dioxide into formic acid. Different ratios of NiCo@rGO catalyst are used to achieve high activity for carbon dioxide reduction reaction to produce formic acid.

A schematic diagram of the preparation of the NiCo@rGO catalyst and the deposition of the catalyst on Sn support using drop-casting method is shown in Fig. 1. Fig. 1 also demonstrates the H-type electrochemical cell, which consists of a cathodic and an anodic compartment separated by an anion exchange membrane (Nafion 117). The cathodic compartment contains $NaHCO_3$ electrolyte as well as reference and working electrodes, while the anodic compartment contains KOH electrolyte and a counter electrode.

## 2. Experimental

### 2.1. Materials

All analytical grade chemicals, including $Ni(NO_3)_2$ (99.7 %), $Co(NO_3)_2$ (99.8 %), $NaHCO_3$ (99.8 %), Ethanol (99 %), Methanol (99 %), $H_2O_2$, NaOH (99.9 %), KOH (99.7 %), and $B_2O_3$ (99.8 %), were used and obtained from Aladin. The Sn foil (99 % pure), and PTFE (poly-

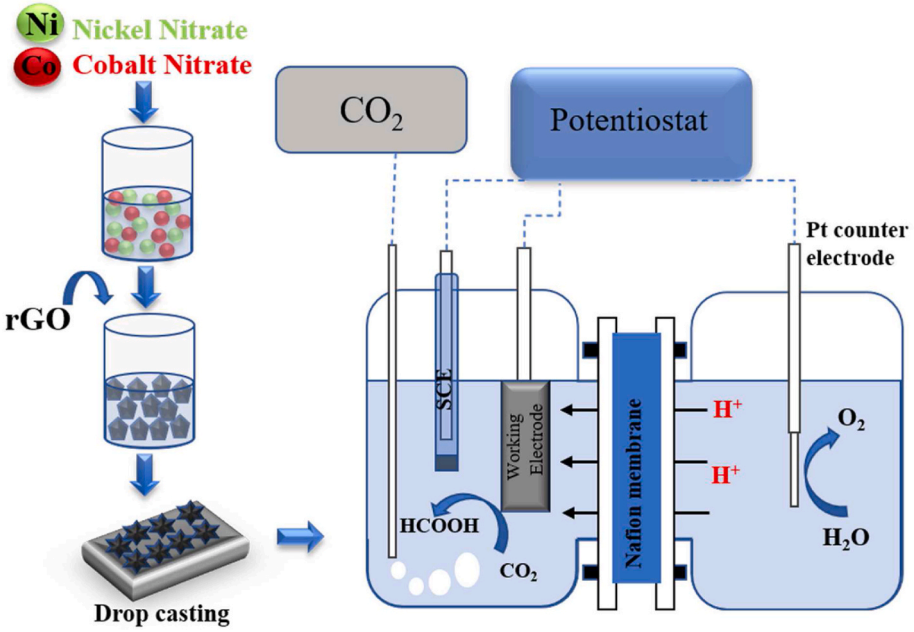


**Fig. 1.** A schematic diagram of the synthesis of colloidal NiCo@rGO catalyst and electrochemical conversion of $CO_2$ into formic acid.

tetrafluoroethylene) were purchased from Sigma-Aldrich. The already prepared rGO was used in catalyst preparation. Deionized water (Millipore system 18.2 MΩ cm at 25 °C) was use for solution preparation and experiments.

### 2.2. Preparation of the colloidal NiCo-based catalyst

The NiCo-based catalyst was prepared using 1 M solution of nickel and cobalt nitrate with a few drops of 0.2 M borate buffer to make colloids. The large size colloidal particles were settled down after a few minutes and removed from the colloidal solution. The rGO support was added to the colloidal NiCo solution and stirred continuously for 30 min to make a homogenous mixture. The NiCo@rGO catalyst was dried at room temperature for a few hours. After that, the precursor was heated at 110 °C to remove any remaining moisture from the catalyst. The black paste of NiCo@rGO was further dried in a furnace at 250 °C for 2 h. The colloidal NiCo@rGO catalyst was ready for further use. Simple Ni and Co based catalysts were also prepared using the above-mentioned procedure.

### 2.3. Preparation of electrodes

The freshly prepared catalysts were deposited on an acid treated Sn electrode using drop-casting method. Before catalyst deposition, the Sn foil (99.95 %) (thickness 0.5 mm) was cut into small electrodes (geometric area of 1 $cm^2$) and rinsed with DI water. The Sn foil was initially treated in 1 M $H_2SO_4$ by applying 3 V for 40 s using the potentiostat. The surface of the Sn foil became rougher during the treatment. The treated Sn foils were sonicated with a mixture of ethanol, acetone, and water to further remove any remaining residues. In the second step, the required amount of catalyst was dissolved in an ethanol/PTFE mixture (100 μl ethanol, 50 μl PTFE) using ultrasonication for 120 min to produce a homogeneous emulsion like ink. In the third step, the Sn foils were rinsed with water and dried in an oven at 100 °C, then catalyst ink was drop-casted on the Sn foils. After coating, the Sn foils were heated at 150 °C for 2 h and then cooled down for 1 h at room temperature. The electrodes were ready for electrochemical investigation.

### 2.4. Physicochemical characterization

The structure of the catalyst was examined using the XRD technique (Bruker D8 Advance Cu ka-40mA, 40 kV, with a 2D Lynx-eye XE PSD counter detector, Germany). The X-ray photoelectron spectroscopy (XPS) (Kratos AXIS Ultra-DLD (Manchester, UK)) was performed to examine the chemical states (C 1s, O 1s, Ni 2p, and Co 2p regions) of the electrocatalysts. Fourier transform infrared (FT-IR) spectrometer for material characterization (Thermo-Scientific Nicolet iS10 (Waltham, Massachusetts, United States)). Transmission Electron Microscopy (TEM) analysis was conducted on the FEI TECNAI G2 STWIN FEG 200 KV (US). Scanning Electron Microscopy (SEM) analysis with energy dispersive X-ray spectroscopy (EDX) and mapping analysis was conducted on Nova Nano SEM 450 (Thermo-Fisher, US) with an accelerating voltage of 10 mA and 10 kV to characterize the chemical compositions and surface morphologies of the catalysts.

### 2.5. Electrochemical measurements

An H-type cell, with its two compartments separated by an anion exchange membrane (Nafion 117) (Fig. 1), was used for the electrochemical studies. The electrochemical cell's cathode consists of a reference (Ag/AgCl) and a working (NiCo@rGO) electrode. The cathodic chamber contains 40 mL of a $NaHCO_3$ electrolyte solution. The Pt counter electrode was placed in the anodic chamber, which contains 40 mL of 1 M KOH electrolyte solution. An aqueous solution of 0.1 M $NaHCO_3$ concentration was used as the cathodic electrolyte, and it was purged with carbon dioxide gas (99.999 %, Linde Gas) at a flow rate of 3 ml/min to achieve a pH of 8.2. A CS2150 potentiostat (Corrtest, China) was used for all of the electrochemical tests. Except for the long-term stability test, all of the electrolysis experiments were conducted for 1 h at a steady current. The product (formic acid) was detected and quantified via HPLC (Shimadzo, LC-2050C LT) using Shim-pack SCR-102H column, with an RID detector, and 0.5 mM perchloric acid as a mobile phase.

## 3. Results and discussion

### 3.1. Materials characterization

The composition of the different catalysts was characterized by Powder X-ray diffraction (PXRD) analysis, and the diffraction patterns were collected at a scanning rate of 2° per minute from 10° to 90° in 2θ. Fig. 2A shows XRD spectra to estimate the broad structure of all catalyst: rGO, Ni, Co, NiCo, and NiCo@rGO. The XRD spectra resemble previously reported data (Ni with PDF # 98-006-9376, Co with PDF # 98-004-9324, NiCo with PDF# 98-006-9377, and NiCo@rGO with PDF# 98-004-3740) [49,50]. The diffraction patterns of colloidal Ni, Co, NiCo, and NiCo@rGO coincide with the above-mentioned references, which are face-centered cubic (FCC) structures. The rGO shows only one broad peak at 35.2°, while other catalysts have multiple diffraction peaks, as reported in the XRD references. The main diffraction peaks of the NiCo@rGO catalyst appears at (220, 111, 311, 400, 511, 422, and 440), which shows that the prepared catalyst is mainly composed of homogenously immersed NiCo material [51]. Fig. 3A shows the XRD spectra of different ratios of NiCo@rGO catalyst. The XRD spectra of $Ni_{0.97}Co_{0.03}$@rGO, $Ni_{0.8}Co_{0.2}$@rGO, $Ni_{0.55}Co_{0.45}$@rGO, $Ni_{0.3}Co_{0.7}$@rGO, and $Ni_{0.13}Co_{0.87}$@rGO were resembled PDF # 98-024-6910, 98-017-381, 98-006-9377, 98-004-3740, and 98-006-9375, respectively. The diffraction peaks of all ratios confirm that the catalysts are mainly composed of homogenously immersed NiCo-based materials.

The prepared catalysts were characterized by SEM (Scanning Electron Microscopy) to reveal the surface morphology, as demonstrated in Fig. 2. Fig. 2B is an SEM image of homogeneously dispersed colloidal Ni nanoparticles. The morphological analysis shows that a homogenously immersed amorphous structure was formed and distributed over the electrode. Fig. 2C is an SEM image of a colloidal Co catalyst, which is similar to the colloidal Ni catalyst. It can be seen that the catalyst is distributed uniformly over the electrode with a nonmetric particle size. The colloidal NiCo catalyst SEM image is shown in Fig. 2D; NiCo homogenously immersed particles are spread all over the electrode, with particle size less than 20 nm. The SEM image of the NiCo@rGO catalyst is shown in Fig. 2E, and its enlarged image is shown in Fig. 2F. The morphological analysis shows that the homogenously immersed particles cover the whole surface of the electrode, and due to the presence of the support, the surface area is enhanced, which may help in electrochemical activity. The SEM images of different ratios of NiCo-based catalysts are shown in Fig. 3B to F. All the different ratio catalysts, $Ni_{0.97}Co_{0.03}$@rGO, $Ni_{0.8}Co_{0.2}$@rGO, $Ni_{0.55}Co_{0.45}$@rGO, $Ni_{0.3}Co_{0.7}$@rGO, and $Ni_{0.13}Co_{0.87}$@rGO, show similar appearance. The catalysts are spread all over the electrodes homogenously with particle size of less than 200 nm. The composition of all the prepared catalyst was confirmed by SEM-EDX and shown in Fig. S1. The EDX of colloidal Ni, Co, NiCo and NiCo@rGO are displayed in Fig. S1, which confirm that colloidal Co catalyst (Fig. S1B) contains mainly Co and colloidal Ni catalyst contains mainly Ni (Fig. S1D), while colloidal NiCo contains both main elements Ni and Co (Fig. S1F). The SEM-EDX spectra of NiCo@rGO catalyst are shown in Fig. S1H. The SEM-EDX spectra of different catalyst ratios are shown in Fig. S2. To further confirm the elements distribution of NiCo@rGO catalyst, SEM-mapping analysis was performed and shown in Fig. 4. The mapping results show that Ni, Co, and C elements are homogenously spread all over the electrode surface. The mapping results of another ratio was shown in Fig. S3, having all the elements Ni, Co, C and O distributed all over the electrode.

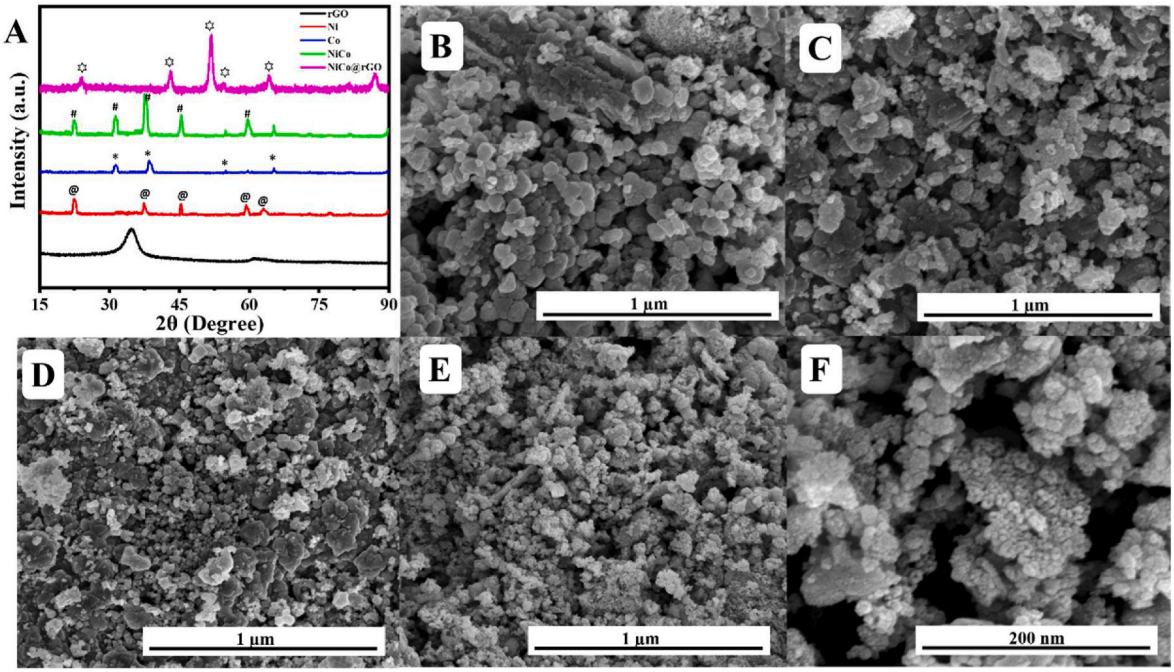


**Fig. 2.** (A) XRD spectra of rGO, colloidal Ni, Co, NiCo and NiCo@rGO catalysts (@, *, # and ☼ are showing the main peaks) while, (B–E) are the SEM images of colloidal Ni, Co, NiCo and NiCo@rGO catalysts, (F) is the enlarge image of NiCo@rGO catalyst.

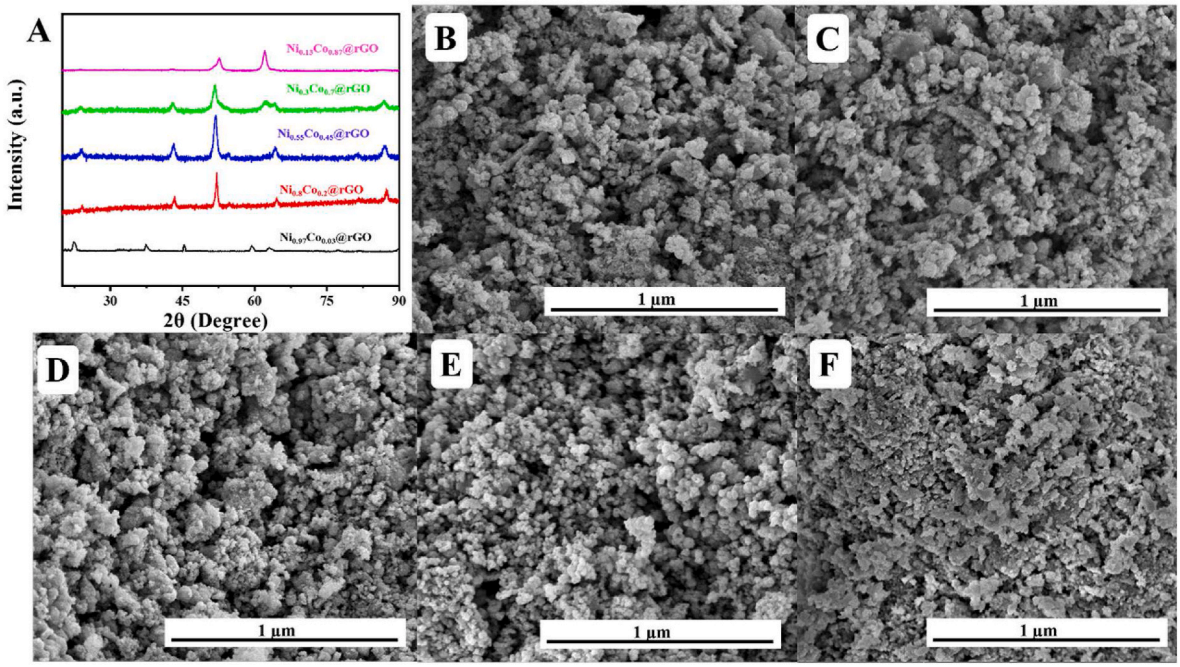


**Fig. 3.** The comparative XPS spectra of different NiCo ratios (A), and the SEM images of $Ni_{0.97}Co_{0.03}$@rGO, $Ni_{0.8}Co_{0.2}$@rGO, $Ni_{0.55}Co_{0.45}$@rGO, $Ni_{0.3}Co_{0.7}$@rGO, and $Ni_{0.13}Co_{0.87}$@rGO (B–F).

The TEM and HRTEM images of the colloidal NiCo@rGO catalyst are displayed in Fig. S4. The presence of NiCo particles embedded on rGO is evident from the micrographs (Fig. S4 a, b). The HRTEM images of NiCo@rGO show a lattice spacing of 0.32 nm (Fig. S4c), with individual particle sizes ranging from 10 to 20 nm. The samples of colloidal NiCo@rGO (Fig. S4d) correspond to the (511), (400), (220), (311), and (111) planes, respectively. Additional confirmation of the homogeneously immersed NiCo@rGO samples was provided through the analysis of selected area electron diffraction (SAED) patterns, as illustrated in Fig. S4d. The SAED patterns of NiCo@rGO material consist of distinct rings that correspond to the NiCo@rGO (440), (111), (220), and (311), respectively. The obtained results are consistent with the XRD spectra of the NiCo@rGO catalyst.

The surface morphology was further characterized by XPS analysis (Fig. 5). The complete XPS spectra of rGO, Ni, Co, NiCo, and NiCo@rGO are shown in Fig. 5A. It has been found that carbon is a major peak in the rGO spectra, Ni has a main peak of Ni element, and Co has a main peak of Co element, while NiCo has peaks of both Ni and Co. The complete

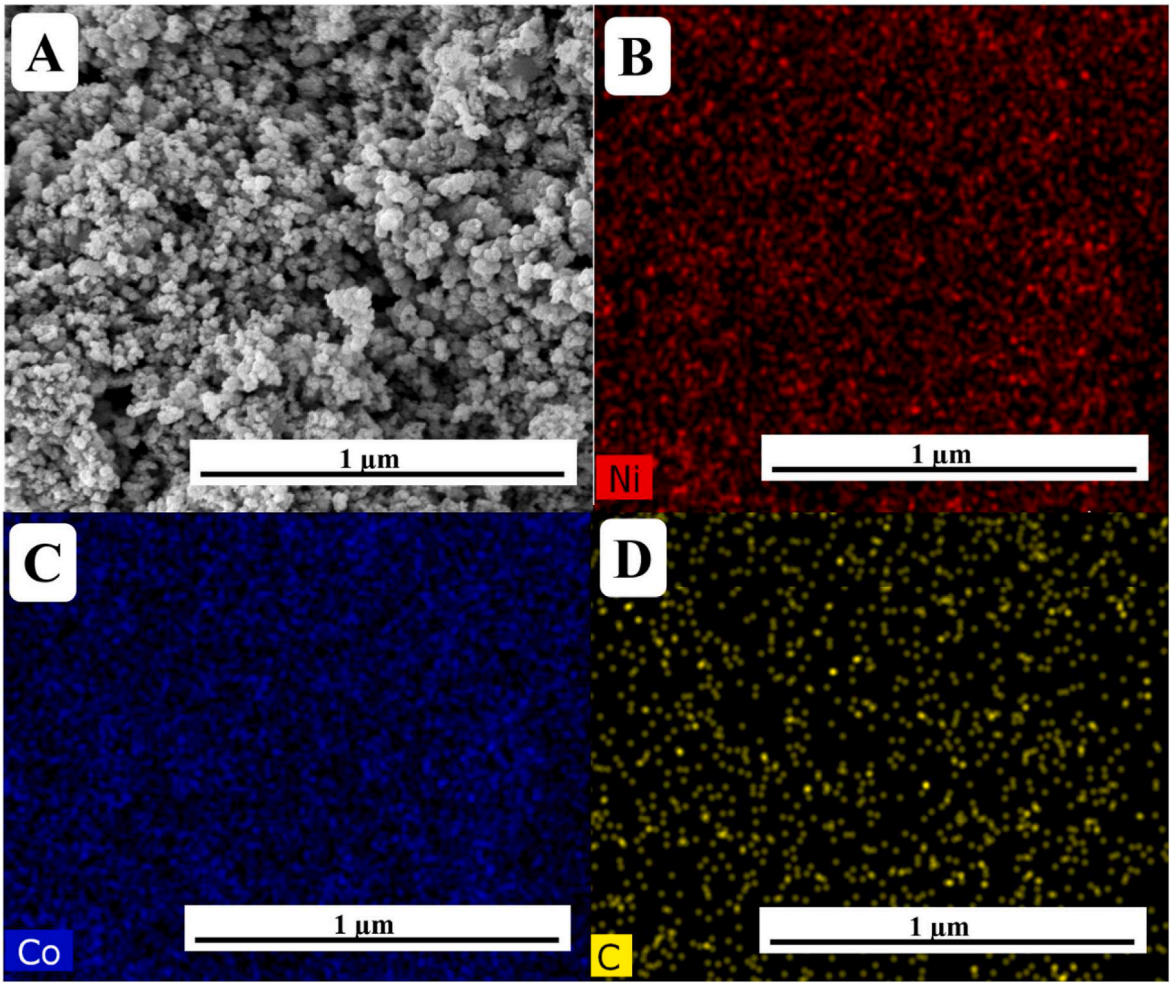


**Fig. 4.** SEM images of NiCo@rGO catalyst (a), with their mapping results of concerned elements Ni (b), Co (c) and C (d).

spectra of NiCo@rGO have all the peaks of C, O, Ni, and Co elements. The XPS spectra of different ratios of NiCo@rGO catalysts are shown in Fig. 5B. The spectra confirm the existence of C, O, Ni, and Co as a prominent peaks. The magnified spectra of the main elements C, O, Co, and Ni are shown in Fig. 5 (C–F). The samples results were calibrated using the binding energy of the C 1s peak at 284.5 eV. For all electrodes, the O1s peaks were observed at 528.6 ± 1 eV. The broad spectra of Co was shown in Fig. 5E having main peaks Co $2p_{1/2}$ and Co $2p_{3/2}$ were observed at 794.3 and 779.2 eV, respectively [52]. The peaks in NiCo complex is slightly shifted from original spectrum (±1 eV), which is due to the formation of colloidal complex.

The broad spectra of Ni in the NiCo complex are illustrated in Fig. 5F, showing that the main peaks of Ni $2p_{1/2}$ and Ni $2p_{3/2}$ were observed at 872.5 and 854 eV, respectively. The shifting of Ni peaks in NiCo colloidal complex is ±1 eV, which is assigned to the formation of the NiCo complex. Through the spectrum of NiCo-based catalyst, the formation of the NiCo composite is confirmed with less than ±1 eV shift in all available peaks, as reported in the literature [49]. The XPS broad spectra of another ratio of NiCo@rGO complex are shown in Fig. S5. The XPS results confirm the formation of the NiCo colloidal complex.

### 3.2. Electrochemical characterization

Electrochemical analysis was performed to investigate the activity of the electrodes for $CO_2$ ECR. Prior to $CO_2$ ECR experiments, LSV experiments were performed to further activate the electrode (at 50 mV/s), as shown in Fig. 6 (A and B). The results suggest that NiCo@rGO based electrodes attained the highest active potential compared to all other electrodes. The LSV experiments of all different ratio of NiCo@rGO were also performed to select the best catalyst. Based on the experimental results, $Ni_{0.55}Co_{0.45}$@rGO attained the highest activity compared to all other ratio of NiCo@rGO based catalysts. The LSV graph of different ratio of NiCo@rGO is shown in Fig. 6B.

The high electron transport capacity and the active sites on electrode surface of NiCo@rGO catalyst have an impact on the electrode electrocatalytic ability. The increase in the electrochemical active surface area (ECSA) often denotes the existence of more active sites on the catalyst's surface [53]. The LSV analysis was carried out at a voltage range of 0 to −2.0 V in order to compare the ECSA of different electrodes. According to the results, NiCo@rGO has the highest $C_{dl}$ value, which suggests that it has more active sites than other electrodes (rGO, Ni, Co and NiCo). The evaluation of the active surface area for each system is achieved by electrochemical means. Specifically, it involves measuring the double-layer charging capacitance of the electrocatalytic surface. The measurement is derived from the non-faradaic region of cyclic voltammetry. Multiple scan rates are employed to generate cyclic voltammograms for analysis. The non-faradaic current is commonly attributed to the charging capacitance of the double-layer (Cdl). This capacitance can be represented by a linear equation, where the slope of the line corresponds to the value of the double-layer charging capacitance, as determined by the following equation.

$$i_c = \nu C_{dl}$$

Where the double-layer charging current is denoted by the symbol $i_c$,

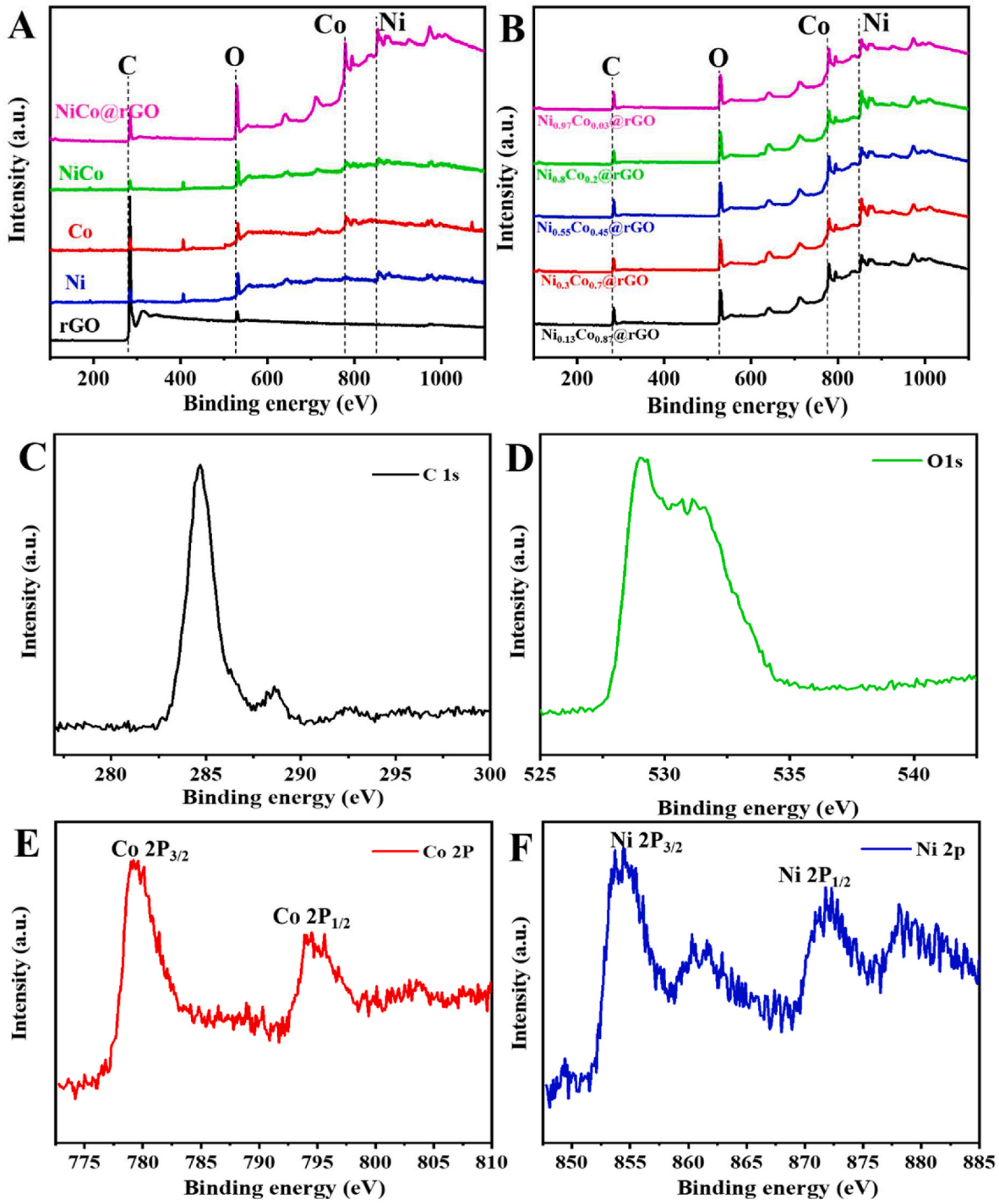


**Fig. 5.** Complete XPS spectra of rGO, Co, Ni, NiCo and NiCo@rGO (A). The complete XPS spectra of different ratio of NiCo@rGO catalyst (B), and separate broad spectra of C, O, Co and Ni (C–F).

and the scan rate and double-layer charging capacitance, respectively, are denoted by $\nu$ and $C_{dl}$. The active surface area is calculated electrochemically by dividing the double-layer capacitance by the specific capacitance of the metal electrode.

$$ECSA = C_{dl}/C_s$$

The capacitance values ($C_s$) of various metal electrodes immersed in alkaline electrolyte solutions, such as NaOH and KOH. In this case, the electrochemically active surface area of NiCo-based electrodes under alkaline conditions was measured, which reports that, NiCo@rGO has the highest ECSA as compared to all other electrodes. To enhance the credibility of the findings, Fourier Transform Infrared spectroscopy was employed. The FTIR spectra of composites and prepared nanoparticles are given in Fig. S7, showing bands with varying modifications. The hydroxyl group is shown in the FT-IR spectrum of the rGO sample at about 3400 $cm^{-1}$ [54]. Interlayer water molecules are responsible for this stretching. The carbonyl groups C═C exhibit aromatic stretching, as indicated by the peaks detected around 1852 $cm^{-1}$ [55]. The presence of functional groups in rGO is confirmed by the peaks around 1700 $cm^{-1}$, which indicate the C–OH functional group. Bending vibrations of nickel and cobalt oxides are responsible for the two characteristic absorption peaks at lower frequencies of 680 $cm^{-1}$ and 720 $cm^{-1}$ observed in NiCo

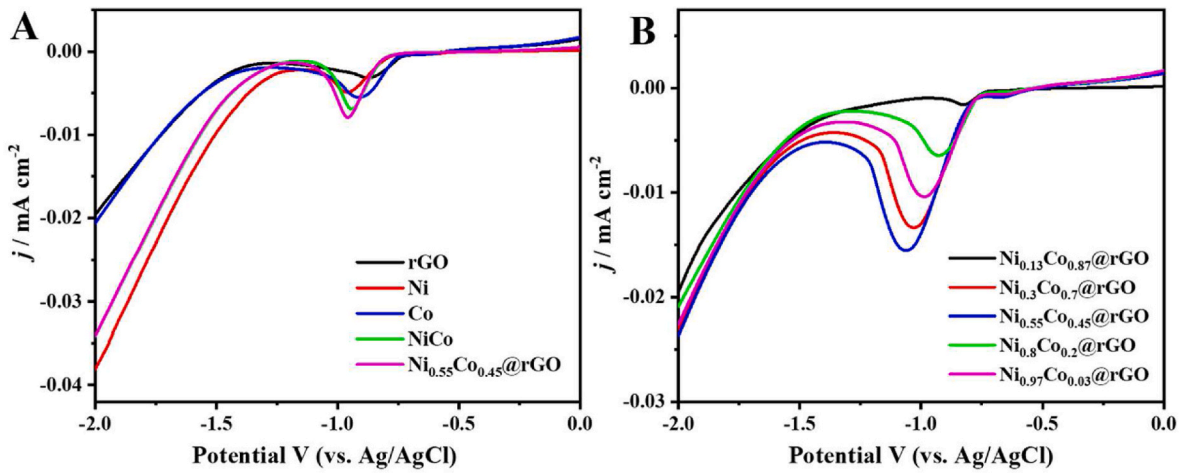


**Fig. 6.** LSV graph of rGO, Ni, Co, NiCo, and NiCo@rGO were shown in (A), while LSV graph of different ratios of NiCo@rGO were also shown (B).

nanoparticles and the remaining components of their composites [54, 55].

To examine the kinetic behaviors of the rGO, Ni, Co, NiCo, and NiCo@rGO electrodes, electrochemical impedance spectroscopy (EIS) analysis was carried out in 0.1 M $NaHCO_3$ electrolyte solution. Fig. S6 illustrates the Nyquist diagrams. The charge transfer properties of the electrode materials are indicated by the Rct (electron transfer resistance) values of the fabricated electrodes. The figure shows the conductivity between the electrodes and the probing species. Fig. S6 depicts the Nyquist plots of the rGO, Ni, Co, NiCo, and NiCo@rGO in a 0.1 M $NaHCO_3$ solution. It is observed that NiCo@rGO attains a very low Rct value (34 Ω) compared to other electrodes. The conductivity of the different catalysts decreases in the following sequence: NiCo@rGO > NiCo > Ni > Co > RGO, which implies that the NiCo@rGO catalyst is a strong contender for the efficient electrochemical analysis approach. The Rct values for rGO, Ni, Co, and NiCo, are decreasing in the following manner 374 Ω, 210 Ω, 180 Ω, 43 Ω, respectively. The NiCo@rGO has the least resistance compared to all other electrodes, which indicates that it has the highest activity. In addition, NiCo@rGO has a unique conductive structure and a remarkable electrical conductivity. These results prove that the interface electron transfer rate is improved from rGO to NiCo@rGO. The reaction kinetics are reduced, and the rapid increase in the $CO_2$ reduction reaction was guaranteed by the NiCo@rGO catalyst. The NiCo@rGO shows better catalytic activity due to the synergetic effect, as mentioned in the previous studies [56].

### 3.3. *Electrocatalytic reduction of $CO_2$*

Multiple electrochemical reduction studies were performed in H-type cells to reveal the electrochemical performance of rGO, Sn foil, Ni, Co, NiCo, and NiCo@rGO catalysts towards $CO_2$ ECR to formic acid. The chronopotentiometry technique was used throughout all studies. The current was kept constant while the potential was changed in chronopotentiometry. All experiments were conducted at a fixed time of 1 h to ensure comparability and consistency. Formic acid concentration was analyzed using High-performance Liquid Chromatography (HPLC) instrument. Experiments were carried out at a constant current of −50 mA and 0.1 M electrolyte concentration. Table 1 displays the results of chronopotentiometry experiments performed with rGO, Ni, Co, NiCo, and NiCo@rGO catalysts at constant current and electrolyte concentration. Multiple runs of the experiments were conducted, and their average values were calculated. The results of formic acid concentrations from multiple experiments are shown in Fig. 8. The role of Sn foil was also evaluated and compared in Table 1.

The experiments were performed to evaluate the results of formic acid and FE at different ratios of NiCo@rGO catalyst. The potential

**Table 1**
A comparison of results at constant initial condition of −50mA and 0.1 M $NaHCO_3$ electrolyte.

| Catalyst | Formic acid Concentration (mg/L) | Faradic Efficiency % |
|---|---|---|
| rGO | 28 | 3 |
| Sn | 89 | 9 |
| Ni | 348 | 32 |
| Co | 326 | 31 |
| NiCo | 487 | 51 |
| NiCo@rGO | 517 | 57 |

spectra of different catalysts are shown in Fig. 7 at constant electrolyte concentrations. Fig. 7B shows the comparison results of chronopotentiometry spectra of different ratios of $Ni_{0.97}Co_{0.03}$@rGO, $Ni_{0.8}Co_{0.2}$@rGO, $Ni_{0.55}Co_{0.45}$@rGO, $Ni_{0.3}Co_{0.7}$@rGO, and $Ni_{0.13}Co_{0.87}$@rGO catalysts at same current value. The chronopotentiometry spectra of $CO_2$ conversion for the tested electrodes at same current value of −50 mA (vs. Ag/AgCl reference electrode) at a fixed time of 1 h are shown in Fig. 7B, and their corresponding results are reported in Table 2. Each experiment was repeated three times to obtain a statistical distribution of the results. The results of electrode FE and formic acid concentration were calculated with a standard deviations of 2 % and 25 mg/L, respectively. The electrode FE shows the dependence on the specific condition of different ratios, as shown in Table 1. $Ni_{0.55}Co_{0.45}$@rGO catalyst attained the highest FE, while $Ni_{0.13}Co_{0.87}$@rGO catalyst acquired the lowest FE. The $Ni_{0.55}Co_{0.45}$@rGO attained the highest FE of about 58 % at −50mA. The energy/power consumption of the electrodes were calculated using Eq. S3 and represented in Table 2. Table 3 illustrates the performance of previously reported catalysts and the developed catalyst in this study for $CO_2$ electrochemical reduction (ECR) to formic acid.

### 3.4. *Long term stability*

The long-term chronopotentiometry experiment was conducted at a constant current of −50 mA in 0.1 M $NaHCO_3$ electrolyte for 10 h to examine the synthesized electrode's long-term stability. Fig. 9 shows the chronopotentiometry spectra of long-term stability. After 10 h, the catalyst showed no signs of destabilization. The average FE was close to 51 %, demonstrating the catalyst's activity and efficiency.

## 4. Conclusions

In this study, a NiCo-based catalyst was successfully prepared using the colloidal method. The NiCo@rGO catalyst was deposited on acid-

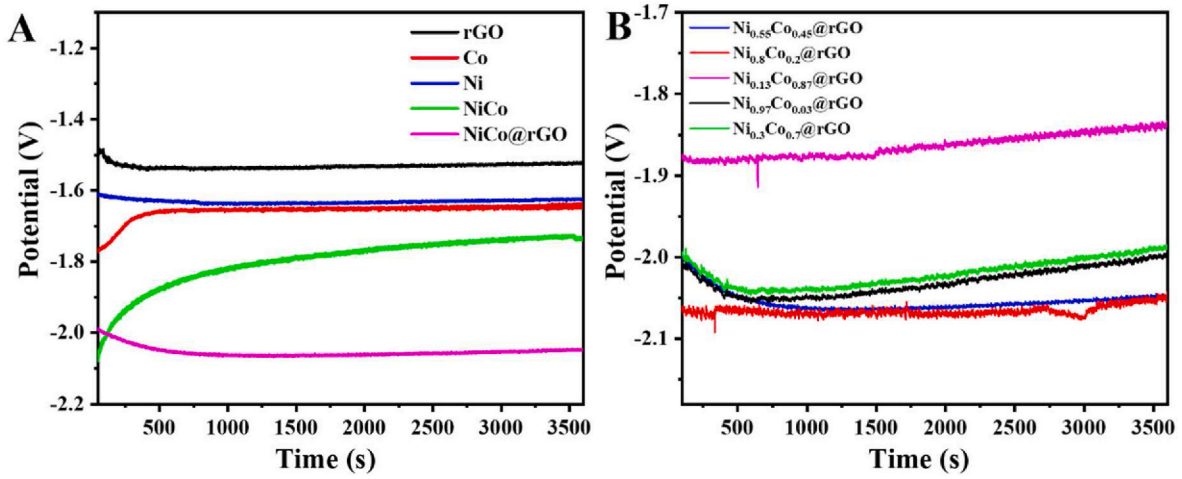


**Fig. 7.** Potential variation of the different materials (rGO, Co, Ni, NiCo and NiCo@rGO) (A), and chronopotentiometry spectra of different ratio of NiCo@rGO based catalysts (B) at fixed conditions.

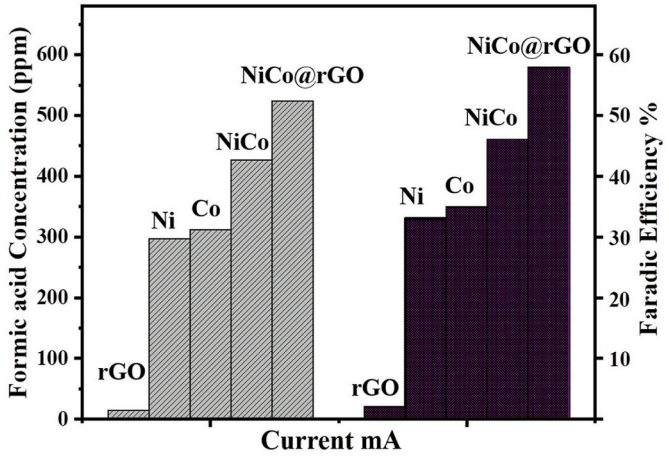


**Fig. 8.** The different catalysts rGo, Ni, Co, NiCo, and NiCo@rGO formic acid concentration and FE at fixed current of −50mA.

**Table 2**
The comparative results of different ratios at constant initial condition of −50mA and 0.1 M $NaHCO_3$ electrolyte.

| Catalyst | Formic acid concentration (mg/L) | Energy consumption ($kWh•mol^{-1}$) | Faradic Efficiency % |
|---|---|---|---|
| $Ni_{0.13}Co_{0.87}$@rGO | 398 | 0.128 | 36 |
| $Ni_{0.3}Co_{0.7}$@rGO | 431 | 0.127 | 42 |
| $Ni_{0.55}Co_{0.45}$@rGO | 524 | 0.106 | 58 |
| $Ni_{0.8}Co_{0.2}$@rGO | 453 | 0.124 | 43 |
| $Ni_{0.97}Co_{0.03}$@rGO | 437 | 0.126 | 42 |

treated Sn electrode using drop-casting method to enhanced activity toward the $CO_2$ reduction reaction. The catalyst was characterized by XRD, SEM, FT-IR, TEM, XPS, EDX, and SEM-Mapping. The analytical technique (Chronopotentiometry) was used for electrochemical $CO_2$ reduction into formic acid. The catalysts of simple metal oxides and different ratios of NiCo@rGO were compared, and the most suitable ratio was selected for the $CO_2$ conversion reaction. The FE values of rGO, Ni, Co, NiCo, and NiCo@rGO electrodes were calculated. The results showed that NiCo@rGO attained the highest FE. The $Ni_{0.55}Co_{0.45}$@rGO catalyst showed the highest FE (58 %) compared to all other catalysts. The electrochemical $CO_2$ conversion experiments of all catalysts were

**Table 3**
Shows the comparative results of previously reported catalyst towards $CO_2$ ECR to formic acid.

| Catalyst | Electrolyte Concentration (M) | Potential (V) | Faradic Efficiency % | References |
|---|---|---|---|---|
| Sn | 0.05 M $KHCO_3$ | −1.48 | 28.5 | [57] |
| In | 0.5 M $K_2SO_4$ | −0.89 | 30 | [58] |
| $SnO_2$/C | 0.1 $KHCO_3$ | −0.9 | 50 | [59] |
| Cu/p-NiO | 0.05 M $K_2CO_3$ | −0.7 vs RHE | 22 | [60] |
| Ni electrode | 0.1 M $KHCO_3$ | −1.19 vs RHE | 23.2 | [61] |
| Ni | 0.05 M $KHCO_3$ | −1.48 vs RHE | 13.7 | [57] |
| $Co_3O_4$ nanofibers | 1 M KOH | −1.7 | 27 | [33] |
| NiCo@rGO | 0.1 M $NaHCO_3$ | −2.1 | 58 | This work |

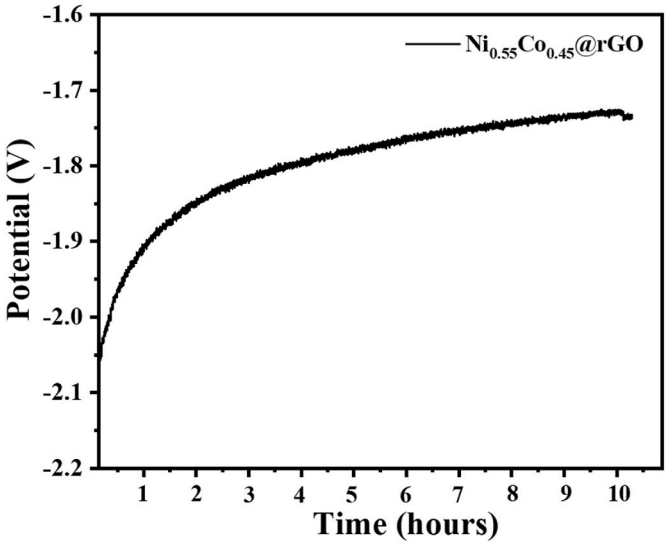


**Fig. 9.** Long term stability of the NiCo@rGO catalyst for a 10 h experimental run with continuous flow of $CO_2$ at constant current in 0.1 M $NaHCO_3$ electrolyte.

performed, and the results were reported. The results confirm the electrochemical conversion of $CO_2$ into formic acid with good activity and high stability. The experimental findings confirm the potential application of the synthesized catalyst in industrial applications.

## CRediT authorship contribution statement

**Muhammad Arsalan:** Conceptualization, Investigation, Methodology, Writing – original draft, Writing – review & editing. **Dina Ewis:** Conceptualization, Data curation, Investigation, Methodology, Writing – original draft. **Muneer M. Ba-Abbad:** Formal analysis, Methodology, Writing – review & editing. **Mazen Khaled:** Formal analysis, Methodology, Writing – review & editing. **Abdulkarem Amhamed:** Project administration, Writing – review & editing. **Muftah H. El-Naas:** Conceptualization, Data curation, Formal analysis, Funding acquisition, Resources, Supervision, Writing – review & editing.

## Declaration of competing interest

The authors declare that they have no known competing financial interests or personal relationships that could have appeared to influence the work reported in this paper.

## Data availability

Data will be made available on request.

## Acknowledgment

The authors would like to acknowledge the support of Qatar National Research Fund (a member of Qatar Foundation) through Grant # NPRP 12 C-33923-SP-102 (NPRP12 C-0821–190017). The findings achieved herein are solely the responsibility of the authors. The authors would like to thank Central Laboratories Unit (CLU) at Qatar University for carrying out SEM and TEM analysis. Open Access funding provided by the Qatar National Library.

## Appendix A. Supplementary data

Supplementary data to this article can be found online at https://doi.org/10.1016/j.rineng.2024.101824.

## References

[1] J. Yuan, M.-P. Yang, W.-Y. Zhi, H. Wang, H. Wang, J.-X. Lu, Efficient electrochemical reduction of $CO_2$ to ethanol on Cu nanoparticles decorated on N-doped graphene oxide catalysts, J. CO2 Util. 33 (2019) 452–460.
[2] O.G. Sánchez, Y.Y. Birdja, M. Bulut, J. Vaes, T. Breugelmans, D. Pant, Recent advances in industrial $CO_2$ electroreduction, Curr. Opin. Green Sustainable Chem. 16 (2019) 47–56.
[3] M. Al Salaheen, W.S. Alaloul, K.M. Alzubi, A.b.A. Malkawi, M.A. Musarat, Advancing waste-based construction materials through carbon dioxide curing: a comprehensive review, Results in Engineering 20 (2023).
[4] D. Ewis, M. Arsalan, M. Khaled, D. Pant, M.M. Ba-Abbad, A. Amhamed, M.H. El-Naas, Electrochemical reduction of $CO_2$ into formate/formic acid: a review of cell design and operation, Separ. Purif. Technol. 316 (2023) 123811.
[5] C. Kim, F. Dionigi, V. Beermann, X. Wang, T. Möller, P. Strasser, Alloy nanocatalysts for the electrochemical oxygen reduction (ORR) and the direct electrochemical carbon dioxide reduction reaction ($CO_2$RR), Adv. Mater. 31 (31) (2019) 1805617.
[6] J. Choi, J. Kim, P. Wagner, S. Gambhir, R. Jalili, S. Byun, S. Sayyar, Y.M. Lee, D. R. MacFarlane, G.G. Wallace, D.L. Officer, Energy efficient electrochemical reduction of $CO_2$ to CO using a three-dimensional porphyrin/graphene hydrogel, Energy Environ. Sci. 12 (2) (2019) 747–755.
[7] A. Hasani, M.A. Teklagne, H.H. Do, S.H. Hong, Q. Van Le, S.H. Ahn, S.Y. Kim, Graphene-based catalysts for electrochemical carbon dioxide reduction, Carbon Energy 2 (2) (2020) 158–175.
[8] B. Ávila-Bolívar, R. Cepitis, M. Alam, J.-M. Assafrei, K. Ping, J. Aruväli, A. Kikas, V. Kisand, S. Vlassov, M. Käärik, J. Leis, V. Ivaništšev, P. Starkov, V. Montiel, J. Solla-Gullón, N. Kongi, $CO_2$ reduction to formate on an affordable bismuth metal-organic framework based catalyst, J. CO2 Util. 59 (2022).
[9] M.A. Hossen, H.M. Solayman, K.H. Leong, L.C. Sim, N. Yaacof, A. Abd Aziz, L. Wu, M.U. Monir, Recent progress in $TiO_2$-Based photocatalysts for conversion of $CO_2$ to hydrocarbon fuels: a systematic review, Results in Engineering 16 (2022).
[10] Y. Deng, Y. Huang, D. Ren, A.D. Handoko, Z.W. Seh, P. Hirunsit, B.S. Yeo, On the role of sulfur for the selective electrochemical reduction of $CO_2$ to formate on CuS (x) catalysts, ACS Appl. Mater. Interfaces 10 (34) (2018) 28572–28581.
[11] M. Zhao, Y. Gu, W. Gao, P. Cui, H. Tang, X. Wei, H. Zhu, G. Li, S. Yan, X. Zhang, Z. Zou, Atom vacancies induced electron-rich surface of ultrathin Bi nanosheet for efficient electrochemical $CO_2$ reduction, Appl. Catal. B Environ. 266 (2020) 118625.
[12] S.A. Al-Tamreh, M.H. Ibrahim, M.H. El-Naas, J. Vaes, D. Pant, A. Benamor, A. Amhamed, Electroreduction of carbon dioxide into formate: a comprehensive review, Chemelectrochem 8 (17) (2021) 3207–3220.
[13] W. Sun, J. Zhu, M. Zhang, X. Meng, M. Chen, Y. Feng, X. Chen, Y. Ding, Recent advances and perspectives in cobalt-based heterogeneous catalysts for photocatalytic water splitting, $CO_2$ reduction, and $N_2$ fixation, Chin. J. Catal. 43 (9) (2022) 2273–2300.
[14] Y.Y. Birdja, J. Vaes, Towards a critical evaluation of electrocatalyst stability for $CO_2$ electroreduction, Chemelectrochem 7 (23) (2020) 4713–4717.
[15] F. Li, Efficient electrochemical reduction of $CO_2$ to formate using Sn-Polyaniline film on Ni foam, Electrochim. Acta 332 (2020) 135457.
[16] W. Wu, S. Shi, Z. Zhang, X. Guo, L. Sun, R. Wei, J. Zhang, L. Gao, X. Pan, G. Xiao, Monodisperse perovskite $CoSn(OH)_6$ in-situ grown on NiCo hydroxide nanoflowers with strong interfacial bonds to boost broadband visible-light-driven photocatalytic $CO_2$ reduction, J. Colloid Interface Sci. 619 (2022) 407–418.
[17] H. Yu, W. Wang, Q. Mao, K. Deng, Z. Wang, Y. Xu, X. Li, H. Wang, L. Wang, Pt single atom captured by oxygen vacancy-rich NiCo layered double hydroxides for coupling hydrogen evolution with selective oxidation of glycerol to formate, Appl. Catal. B Environ. 330 (2023) 122617.
[18] D. Li, R. Xu, R.J. Wong, X. Zhu, D. Tian, L. Jiang, Q. Guo, H. Bai, L. Huang, W. Liu, H. Wang, K. Li, Suppressing byproduct formation for high selective $CO_2$ reduction over optimized Ni/$TiO_2$ based catalysts, J. Energy Chem. 72 (2022) 465–478.
[19] R. Gonçalves, S. Lanceros-Méndez, C.M. Costa, Electrode fabrication process and its influence in lithium-ion battery performance: state of the art and future trends, Electrochem. Commun. 135 (2022).
[20] M. Arsalan, D. Ewis, N. Mahmud, M.M. Ba-Abbad, M. Khaled, M.H. El-Naas, Enhanced electrochemical conversion of $CO_2$ into formic acid using $PbSO_4$/AtSn electrode: catalyst synthesis and process optimization, J. Environ. Chem. Eng. 11 (6) (2023) 111325.
[21] S. Zhang, P. Kang, S. Ubnoske, M.K. Brennaman, N. Song, R.L. House, J.T. Glass, T. J. Meyer, Polyethylenimine-enhanced electrocatalytic reduction of $CO_2$ to formate at nitrogen-doped carbon nanomaterials, J. Am. Chem. Soc. 136 (22) (2014) 7845–7848.
[22] T. Gunji, H. Ochiai, Y. Isawa, Y. Liu, F. Nomura, M. Miyauchi, F. Matsumoto, Electrocatalytic conversion of carbon dioxide to formic acid over nanosized $Cu_6Sn_5$ intermetallic compounds with a $SnO_2$ shell layer, Catal. Sci. Technol. 9 (23) (2019) 6577–6584.
[23] M.A. Hossen, H.M. Solayman, K.H. Leong, L.C. Sim, N. Yaacof, A. Abd Aziz, L. Wu, M.U. Monir, Recent progress in $TiO_2$-Based photocatalysts for conversion of $CO_2$ to hydrocarbon fuels: a systematic review, Results in Engineering 16 (2022) 100795.
[24] D. Li, J. Wu, T. Liu, J. Liu, Z. Yan, L. Zhen, Y. Feng, Tuning the pore structure of porous tin foam electrodes for enhanced electrochemical reduction of carbon dioxide to formate, Chem. Eng. J. 375 (2019) 122024.
[25] G. Liu, S.M. Ciborowski, Z. Zhu, Y. Chen, X. Zhang, K.H. Bowen, The metallo-formate anions, $M(CO_2)-$, M = Ni, Pd, Pt, formed by electron-induced $CO_2$ activation, Phys. Chem. Chem. Phys. 21 (21) (2019) 10955–10960.
[26] F. Guo, G. He, Size, alloy and interface effects on Cu-based catalysts for enhancing electrochemical reduction of $CO_2$, Results in Engineering 20 (2023) 101510.
[27] B. Ávila-Bolívar, V. Montiel, J. Solla-Gullón, Electrochemical reduction of $CO_2$ to formate on nanoparticulated Bi−Sn−Sb electrodes, Chemelectrochem 9 (9) (2022).
[28] S. Abner, A. Chen, Design and mechanistic study of advanced cobalt-based nanostructured catalysts for electrochemical carbon dioxide reduction, Appl. Catal. B Environ. 301 (2022) 120761.
[29] M. Arsalan, I. Saddique, M. Baoji, A. Awais, I. Khan, M.A. Shamseldin, S. Mehrez, Novel synthesis of sensitive Cu-ZnO nanorod–based sensor for hydrogen peroxide sensing, Front. Chem. (2022) 700.
[30] S.E. Lee, A. Nasirian, Y.E. Kim, P.T. Fard, Y. Kim, B. Jeong, S.-J. Kim, J.-O. Baeg, J. Kim, Visible-Light photocatalytic conversion of carbon dioxide by Ni(II) complexes with $N_4S_2$ coordination: highly efficient and selective production of formate, J. Am. Chem. Soc. 142 (45) (2020) 19142–19149.
[31] X. Kong, Y. Liu, P. Li, J. Ke, Z. Liu, F. Ahmad, W. Yan, Z. Li, Z. Geng, J. Zeng, Coordinate activation in heterogeneous carbon dioxide reduction on Co-based molecular catalysts, Appl. Catal. B Environ. 268 (2020) 118452.
[32] F. Guo, G. He, Size, alloy and interface effects on Cu-based catalysts for enhancing electrochemical reduction of $CO_2$, Results in Engineering 20 (2023).
[33] A. Aljabour, H. Coskun, D.H. Apaydin, F. Ozel, A.W. Hassel, P. Stadler, N. S. Sariciftci, M. Kus, Nanofibrous cobalt oxide for electrocatalysis of $CO_2$ reduction to carbon monoxide and formate in an acetonitrile-water electrolyte solution, Appl. Catal. B Environ. 229 (2018) 163–170.
[34] X. Zhang, S.-X. Guo, K.A. Gandionco, A.M. Bond, J. Zhang, Electrocatalytic carbon dioxide reduction: from fundamental principles to catalyst design, Materials Today Advances 7 (2020) 100074.
[35] Z. Zhang, X.E. Verykios, S.M. MacDonald, S. Affrossman, Comparative study of carbon dioxide reforming of methane to synthesis gas over Ni/$La_2O_3$ and conventional nickel-based catalysts, J. Phys. Chem. 100 (2) (1996) 744–754.

[36] G. Díaz-Sainz, K. Fernández-Caso, T. Lagarteira, S. Delgado, M. Alvarez-Guerra, A. Mendes, A. Irabien, Coupling continuous $CO_2$ electroreduction to formate with efficient Ni-based anodes, J. Environ. Chem. Eng. 11 (1) (2023) 109171.
[37] X. Su, X.-F. Yang, Y. Huang, B. Liu, T. Zhang, Single-Atom catalysis toward efficient $CO_2$ conversion to CO and formate products, Accounts Chem. Res. 52 (3) (2019) 656–664.
[38] P. Zafari, A. Ghaemi, Modeling and optimization of $CO_2$ capture into mixed MEA-PZ amine solutions using machine learning based on ANN and RSM models, Results in Engineering 19 (2023) 101279.
[39] M. Li, X. Deng, Y. Liang, K. Xiang, D. Wu, B. Zhao, H. Yang, J.-L. Luo, X.-Z. Fu, CoxP@NiCo-LDH heteronanosheet arrays as efficient bifunctional electrocatalysts for co-generation of value-added formate and hydrogen with less-energy consumption, J. Energy Chem. 50 (2020) 314–323.
[40] M. Arsalan, A. Awais, X. Qiao, Q. Sheng, J. Zheng, Preparation and comparison of colloid based $Ni_{50}Co_{50}(OH)_2$/BOX electrocatalyst for catalysis and high performance nonenzymatic glucose sensor, Microchem. J. 159 (June) (2020), 105486-105486.
[41] M.A. Rodriguez-Olguin, C. Flox, R. Ponce-Pérez, R. Lipin, F. Ruiz-Zepeda, J. P. Winczewski, T. Kallio, M. Vandichel, J. Guerrero-Sánchez, J.G.E. Gardeniers, N. Takeuchi, A. Susarrey-Arce, Chlorine in NiO promotes electroreduction of $CO_2$ to formate, Appl. Mater. Today 28 (2022) 101528.
[42] Z. Li, D. He, X. Yan, S. Dai, S. Younan, Z. Ke, X. Pan, X. Xiao, H. Wu, J. Gu, Size-dependent nickel-based electrocatalysts for selective $CO_2$ reduction, Angew Chem. Int. Ed. Engl. 59 (42) (2020) 18572–18577.
[43] Z. Zhao, Z. Chen, G. Lu, Computational discovery of nickel-based catalysts for $CO_2$ reduction to formic acid, J. Phys. Chem. C 121 (38) (2017) 20865–20870.
[44] J. Du, Y. Han, H. Zhang, X. Gao, J. Guan, A. Chen, $CoP_2O_6$-assisted copper/carbon catalyst for electrocatalytic reduction of $CO_2$ to formate, ACS Nano 17 (11) (2023) 10055–10064.
[45] H. Liu, Z. Wang, B. Pan, M. Li, S. Huang, J.H. Lee, N.H. Kim, Carbon felt/nitrogen-doped graphene/paraffin wax 3D skeleton regulated tribological performances of the MCPA6 composites: a novel strategy of oil embedding and transporting, Tribol. Int. 184 (2023).
[46] X. Kong, J. Ke, Z. Wang, Y. Liu, Y. Wang, W. Zhou, Z. Yang, W. Yan, Z. Geng, J. Zeng, Co-based molecular catalysts for efficient $CO_2$ reduction via regulating spin states, Appl. Catal. B Environ. 290 (2021) 120067.
[47] J. Du, A. Chen, Ni nanoparticles confined by yolk-shell structure of CNT-mesoporous carbon for electrocatalytic conversion of $CO_2$: switching CO to formate, J. Energy Chem. 70 (2022) 224–229.
[48] Q. Huang, H. Liu, W. An, Y. Wang, Y. Feng, Y. Men, Synergy of a metallic NiCo dimer anchored on a $C_2N$–graphene matrix promotes the electrochemical $CO_2$ reduction reaction, ACS Sustain. Chem. Eng. 7 (23) (2019) 19113–19121.
[49] J. Dong, T. Sun, Y. Zhang, H. Zhang, S. Lu, D. Hu, J. Chen, L. Xu, Mesoporous NiCo alloy/reduced graphene oxide nanocomposites as efficient hydrogen evolution catalysts, J. Colloid Interface Sci. 599 (2021) 603–610.
[50] R. Fazel Zarandi, B. Rezaei, H.S. Ghaziaskar, A.A. Ensafi, Modification of copper electrode with copper nanoparticles@ reduced graphene oxide–Nile blue and its application in electrochemical $CO_2$ conversion, Mater. Today Energy 18 (2020) 100507.
[51] S. Zhang, Q. Fan, R. Xia, T.J. Meyer, $CO_2$ reduction: from homogeneous to heterogeneous electrocatalysis, Accounts Chem. Res. 53 (1) (2020) 255–264.
[52] M. Usman, M. Humayun, M.D. Garba, L. Ullah, Z. Zeb, A. Helal, M.H. Suliman, B. Y. Alfaifi, N. Iqbal, M. Abdinejad, A.A. Tahir, H. Ullah, Electrochemical reduction of $CO_2$: a review of cobalt based catalysts for carbon dioxide conversion to fuels, Nanomaterials 11 (8) (2021) 2029.
[53] L. Li, A. Ozden, S. Guo, A.d.A.F.P. Garci, C. Wang, M. Zhang, J. Zhang, H. Jiang, W. Wang, H. Dong, D. Sinton, E.H. Sargent, M. Zhong, Stable, active $CO_2$ reduction to formate via redox-modulated stabilization of active sites, Nat. Commun. 12 (1) (2021) 5223.
[54] J. Rashid, K. Gilani, A. Arif, C.S. Saraj, W. Li, M. Xu, Facile synthesis of NiCo@rGO as bifunctional electrocatalyst for enhanced water splitting, Int. J. Hydrogen Energy 51 (2024) 774–786.
[55] G. Marimuthu, G. Palanisamy, T. Pazhanivel, G. Bharathi, K.P. Tiruppathi, D. Nataraj, $NiCo_2O_4$ functionalized with rGO catalyst as an active layer for ammonia sensing, Ionics 26 (10) (2020) 5233–5240.
[56] O.I. Metwalli, W. Eisa, B. Anis, A.N.M. Salem, A.S.G. Khalil, M.M.H. Khalil, High performance Ni nanoparticles@Graphene oxide-crosslinked poly(vinyl alcohol) free-standing film for catalytic applications: reductive and oxidative reactions, J. Mater. Res. Technol. 20 (2022) 1142–1156.
[57] M. Azuma, K. Hashimoto, M. Hiramoto, M. Watanabe, T. Sakata, Electrochem. Soc 137 (1990) 1772.
[58] Z.M. Detweiler, J.L. White, S.L. Bernasek, A.B. Bocarsly, Anodized indium metal electrodes for enhanced carbon dioxide reduction in aqueous electrolyte, Langmuir 30 (25) (2014) 7593–7600.
[59] Z. Wang, C. Yang, A. Guan, L. Shang, A.M. Al-Enizi, L. Zhang, G. Zheng, Sub-5 nm $SnO_2$ chemically coupled hollow carbon spheres for efficient electrocatalytic $CO_2$ reduction, J. Mater. Chem. A 6 (41) (2018) 20121–20127.
[60] J.S. DuChene, G. Tagliabue, A.J. Welch, X. Li, W.-H. Cheng, H.A. Atwater, Optical excitation of a nanoparticle Cu/p-NiO photocathode improves reaction selectivity for $CO_2$ reduction in aqueous electrolytes, Nano Lett. 20 (4) (2020) 2348–2358.
[61] A. Kudo, S. Nakagawa, A. Tsuneto, T. Sakata, Electrochemical reduction of high pressure $CO_2$ on Ni electrodes, J. Electrochem. Soc. 140 (6) (1993) 1541.